

# **Periodic linear complexions: Co-segregation of solutes at a low-angle grain boundary in a magnesium alloy**

Risheng Pei<sup>1\*</sup>, Zhuocheng Xie<sup>1\*</sup>, Achraf Atila<sup>2</sup>, Simon Anoldi<sup>1</sup>, Lei Xiao<sup>3</sup>, Xiaoqing Liu<sup>4</sup>, Hexin Wang<sup>1</sup>, Sandra Korte-Kerzel<sup>1</sup>, Julien Guérolé<sup>5</sup>, Talal Al-Samman<sup>1</sup>

<sup>1</sup> Institut für Metallkunde und Materialphysik, RWTH Aachen University, 52056 Aachen, Germany

<sup>2</sup> Department of Materials Science and Engineering, Saarland University, 66123 Saarbrücken, Germany

<sup>3</sup> College of Materials Science and Engineering, Fuzhou University, 350108 Fuzhou, China

<sup>4</sup> School of Physics and Electronics, Gannan Normal University, 341000 Ganzhou, China

<sup>5</sup> Université de Lorraine, CNRS, Arts et Métiers, LEM3, 57070 Metz, France

## **Abstract**

Solute segregation at low angle grain boundaries (LAGB) in Mg alloys significantly affects GB energy and mobility, therefore recrystallization kinetics and corresponding texture modification. In a system featuring multiple substitutional elements at high local concentration levels, solute-solute interaction needs to be considered to interpret and predict co-segregation behavior. In this work, atomic-scale experimental and modelling techniques were applied to investigate the co-segregation behavior of Ca, Zn and Al solutes at a LAGB in a Mg alloy. Three-dimensional atom probe tomography and corresponding clustering analysis revealed a strong clustering tendency of Ca solutes at the linear dislocation arrays. Atomistic simulations indicate that the co-segregation of Ca-Ca pairs in vicinity of the dislocation core region is more

energetically favorable than other solute pairs, as well as the segregation of individual solutes.

**Keywords:** atom probe tomography, atomistic simulation, grain boundary, co-segregation, magnesium alloy

## 1 Introduction

Recrystallization is of great significance of the texture modification for Magnesium alloys [1-3]. Recrystallization can be divided into dynamic and static recrystallization [4-7]. Dependent on the mechanisms, dynamic recrystallization can be further divided into continuous and discontinuous dynamic recrystallization. For the former case, recrystallization initiates by the continuously sub-grain rotation in the vicinity of the deformation zone (e.g. shear bands, deformation bands, transition bands and grain boundary) [4, 6, 8, 9], formed by dislocation attraction during deformation in the matrix. In the latter case, recrystallization initiates by nucleation and growth [6, 7]. In the process of nucleation, low angle grain boundary (LAGB) is formed by dynamic dislocation recovery and the movement of LAGB swept more and more dislocations in the deformed matrix [6]. In this way, the misorientation angle of the boundary keeps increasing to form a high angle grain boundary (HAGB), namely incubation of nucleation. In this stage, solute atoms were proved to slow down the mobility of LAGB to prolong incubation time and restrict recrystallization kinetics [10-13]. According to [10-12], LAGB moves by vacancy-mediated climb of dislocations. According to the mechanism, a LAGB is pinned by extrinsic dislocations, introduced by external forces during deformation, and vacancies are necessary to free the external dislocations by enabling them to climb [10-12]. Therefore, additional driving force is necessary to release the vacancy attracted by solute atoms segregated on the LAGB [10-12]. The fundamental understanding of the segregation behavior of solute atoms at LAGB is

critical for the fully unraveling of the recrystallization mechanisms of dynamic recrystallization.

Recently, solute segregation behaviors on at symmetrical tilt grain boundaries (GBs) and twin boundaries were investigated using high-resolution transmission microscopy (HRTEM) with aberration correction. Periodical segregation patterns of Gd and Nd atoms are clearly evidenced by bright Z-contrast [14-18]. Nie *et al.* reported the periotic segregation of Gd and Zn at tension twin boundary could evidently pinned their motion and strengthen the material [17]. Solute clusters of a few nanometers size were observed segregated at large-angle general GBs in a Mg-Gd alloy [19]. Besides GB segregation, precipitation of binary quasicrystals containing crystal building blocks of topologically close-packed phases was observed at the edge dislocations in Mg-Zn alloys [20]. However, it is hard to avoid the influence of neighboring matrix for the chemical characterization in TEM. In addition, TEM analysis is limited on 2D so that 3D information of GBs and the solute atoms decorated on them are missing.

Atomic-scale modelling techniques were widely used to investigate substitutional segregation behavior at GBs, specifically by calculating segregation energy at the GB sites. Using density functional theory (DFT), per-site segregation energies of multiple alloy elements at coincident site lattice (CSL)  $\Sigma 7$  GB and tension and compression twin boundaries in Mg were calculated [21, 22]. By combining atomistic simulations with machine learning approaches, the effects of GB structure and local atomic environment on the per-site segregation energies of Al solute at  $\langle 0001 \rangle$  symmetric tilt GBs in Mg were explored [23]. Recently, the authors investigated the inhomogeneous segregation behavior of Nd solute at general GBs in Mg using atomistic simulations based on the experimentally informed crystallographic orientation relationships [24]. However, all of these works were conducted in the spirit of the

Langmuir-McLean isotherm [25] in infinitesimally diluted systems, without considering solute-solute interactions when concentration levels are high. So far, the co-segregation behavior of solute elements at GBs in chemical complex alloys is barely investigated in atomic-scale. Only a few DFT studies reported the co-segregation of one or two elements at a limited number of sites in CSL GBs [26-29]. Understanding the co-segregation behavior of more general GBs requires extensive involvement of a much larger number of GB sites and their combinations, thus demanding significantly more computational resources, particularly in terms of DFT accuracy. In addition, this approach applied to CSL GBs was questioned due to the limited number of GB sites in these high-symmetry GBs cannot capture the full spectrum of local atomic environments in general GBs, leading to incorrect structure-property relationships [30].

In this work, we investigated the co-segregation behavior of multiple solute elements at a LAGB in a chemical complex Mg alloy, utilizing a combination of atomic-scale experimental techniques and atomistic simulations. Three-dimensional atom probe tomography (APT) and clustering analysis revealed significant tendencies for clustering of solutes surrounding the microstructural line defects. Correlative atomistic simulations further elucidated the co-segregation behavior of solute-solute pairs at these defects.

## **2 Experimental and simulation methods**

The studied material was an extruded Mg-0.23 wt.% Al-1.00 wt.% Zn- 0.38 wt.% Ca alloy. After gravity casting and homogenization treatment (420 °C×24 hrs), inductively coupled plasma-optical emission spectrometry (ICP-OES) was used to characterize the alloy composition. The alloy was machined into extrusion billets with a diameter  $D_0 = 45$  mm. Hot extrusion was then carried out at 250 °C with a speed of 1.0 mm/s producing extruded bars of  $D_f = 9.0$  mm in diameter, which corresponds to

an extrusion ratio of  $\sim 1:25$  and a logarithmic strain of 3.22 calculated by  $\ln(D_0/D_f)^2$ . The microstructure of the as-extruded sample consists of large elongated grains along ED and small recrystallized grains with an average grain size of 3.2  $\mu\text{m}$  as shown in Fig. S 1. According to the IPF color coding, the deformed grains aligned  $[10\bar{1}0]$  axis parallel to the extrusion direction (ED), while the recrystallized grains are random orientated, revealing the texture modification effect by DRX during extrusion.

An APT tip was lifted out in a deformed grain to investigate the segregation behavior of the solute atoms at LAGB by transmission Kikuchi diffraction (TKD)-assisted focused ion beam (FIB) milling in a FEI Helios 600i dual-beam electron microscope. Details of this method can be found in [24]. 3D atom probe tomography (APT) in a Local Electrode Atom Probe 4000X HR from Cameca was employed to quantify the chemical composition of six general GBs using laser-pulsing mode at a temperature of 30 K. Reconstruction of the evaporated tips was performed using the software package IVAS 3.8.2. Correlative atomistic simulations to investigate the relationship between per-site segregation energy and the local site environment were performed using the open-source MD software package LAMMPS [31] in conjunction with the modified embedded atom method (MEAM) potential for MgCaZn [32], MgCaAl and MgZnAl [33]. The atomistic configurations of symmetric tilt GBs were constructed using the open source tool AtomsK [34] based on experimentally determined crystallographic orientations of the GB plane and related grains obtained from TKD mapping and reconstructed APT tip.

### **3 Results and discussion**

The TKD map before the last milling step was shown in Fig. 1 (a). To illustrate the lattice distortion in the deformed matrix, the inverse pole figure (IPF) color key in the map was restricted to  $5^\circ$  with reference to the average orientation of the whole map.

The position of the final APT tip and the GB were outlined in Fig. 1 (a). The orientations and the GB characteristics ( $1.08^\circ$   $[\bar{1}10\bar{2}]$  on  $(11\bar{2}0)$  GB plane) can be derived from the TKD results. Fig. 1 (b) presents the elemental distribution maps of Mg, Ca, Zn and Al atoms from the reconstructed APT tip containing the LAGB, and the enrichment of Ca, Zn and Al atoms at the planar defect was observed. The linear segregations on the GB can be observed clearly from the top view of the tip as shown in Fig. 1 (d). The corresponding orientation from the top view and the  $\{10\bar{1}0\}$  plane traces were calculated according the Euler orientation measured by TKD presented in Fig. 1 (c). The segregation lines measured from APT are evidently parallel to one of the  $\{10\bar{1}1\}$  plane traces, indicating the segregation lines lie on  $(1\bar{1}01)$  plane. On the premise, these segregation lines should be along the intersection line between  $(1\bar{1}01)$  and  $(11\bar{2}0)$ , namely  $[\bar{1}102]$ .

The concentration profile at GB across the segregating lines were extracted from a cylindrical region of interest with diameter of 30 nm as outlined in Fig. 1 (d) and the results are plotted in Fig. 1 (e). A pronounced periodic line segregation of solutes, especially Ca, at the LAGB was observed with a specific spacing of  $18.7 \pm 0.2$  nm, (Fig. 1 (e)). The peak concentrations of Ca, Zn and Al on the lines and the neighboring region at GB of four lines are listed in Table 1. The measured Ca, Zn and Al average peak concentrations at the LAGB were 1.29, 1.10 and 0.70 at.%, respectively. It is evident that Ca atoms exhibited a much stronger segregation potential with segregation ratio of 12.56, while Zn and Al showed a similar segregation potential with a segregation ratio around 4.65 to 4.05, respectively. This result can be better visualized on the iso-surface maps as shown in Fig. 2 (a-c), where the thresholds were 1.0, 1.2 and 0.8 at.% iso-concentrations for Ca, Zn and Al, respectively. This line feature is suspected to be an edge-like dislocation array as the measured

misorientation angle in alignment with the prediction of Frank-Bilby relation [35-37] based on the distance between edge dislocations in a pure tilt GB:  $\theta = 2 \arcsin \frac{b}{2d} = 0.98 \pm 0.2^\circ$ ; given  $b = 0.32$  nm.

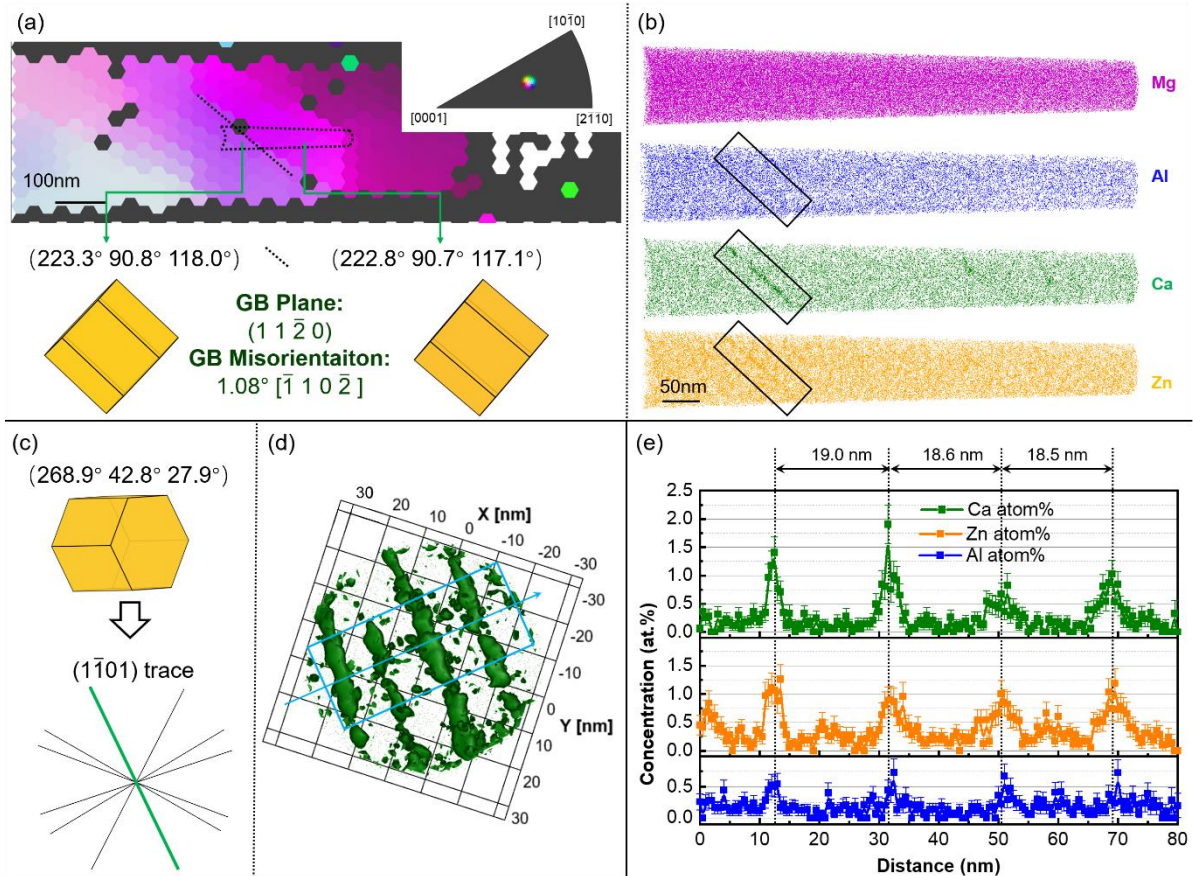


Fig. 1 Reconstructed 3D APT tip of the AZX alloy with a segment of a detected GB milled by guidance of TKD [24]: (a) TKD mapping during tip milling, colored with IPF color key with a deviation of  $5^\circ$  from the average points, indicating the LAGB with a misorientation of  $1.08^\circ$   $[\bar{1}10\bar{2}]$  on the  $(11\bar{2}0)$  plane. (b) Elemental distributions of Mg, Al, Ca and Zn, showing the segregation of Al, Ca and Zn on the bottom of the tip. (c) Unit cell of the tip from top view and the corresponding  $(1\bar{1}01)$  plane trace. (d) Ca atom overlaid with 1.0 at.% Ca iso-surfaces on the top within the region of interest marked in (b), indicating the line segregation structure on the LAGB. (e) Concentration profile on the GB across the segregating lines, extracted from a cylindrical ROI 1 (diameter of 30 nm) outlined in (d), illustrating the periodic segregation of Ca, Zn and Al with a spacing of  $18.7 \pm 0.2$  nm.

Table 1 Comparisons of the concentrations of Ca, Zn and Al on the periodic segregation lines and the neighboring region at the LAGB.

Position	Ca		Zn		Al	
	Peak	Neighbor	Peak	Neighbor	Peak	Neighbor
#1	1.43	0.14	1.27	0.22	0.59	0.16
#2	1.92	0.11	0.95	0.30	0.76	0.15
#3	0.78	0.06	1.02	0.22	0.68	0.14
#4	1.02	0.10	1.14	0.34	0.76	0.15
Mean	1.29	0.10	1.10	0.27	0.70	0.15
Deviation	0.39	0.02	0.11	0.05	0.06	0.005
Segregation ratio	12.56		4.05		4.65	

Clustering ratio  $R$  was employed to assess the clustering tendency of solute elements in the APT-reconstructed sample of the chemical complex Mg alloy. The definition of clustering ratio can be found in the Supplementary. Fig. 2 (c-d) shows the  $R_{X-X}$  and  $R_{X-Y}$  values for both the GB (dashed lines) and bulk (solid lines) regions, with the values varying dependent on the sampling radius. As the sampling radius increases, the  $R$  values decrease and eventually converge to 1 in the bulk regions, indicating a homogeneous distribution when a sufficiently large space is sampled. In addition, the  $R$  values for the GB regions are consistently higher than those for the bulk regions, suggesting a stronger clustering tendency of solute atoms at the GB. Notably, the  $R_{Ca-Ca}$  value at the GB is significantly higher than that of other solute-solute pairs at all sampling radii, which implies a stronger clustering tendency of Ca solutes compared to other solutes at the LAGB.



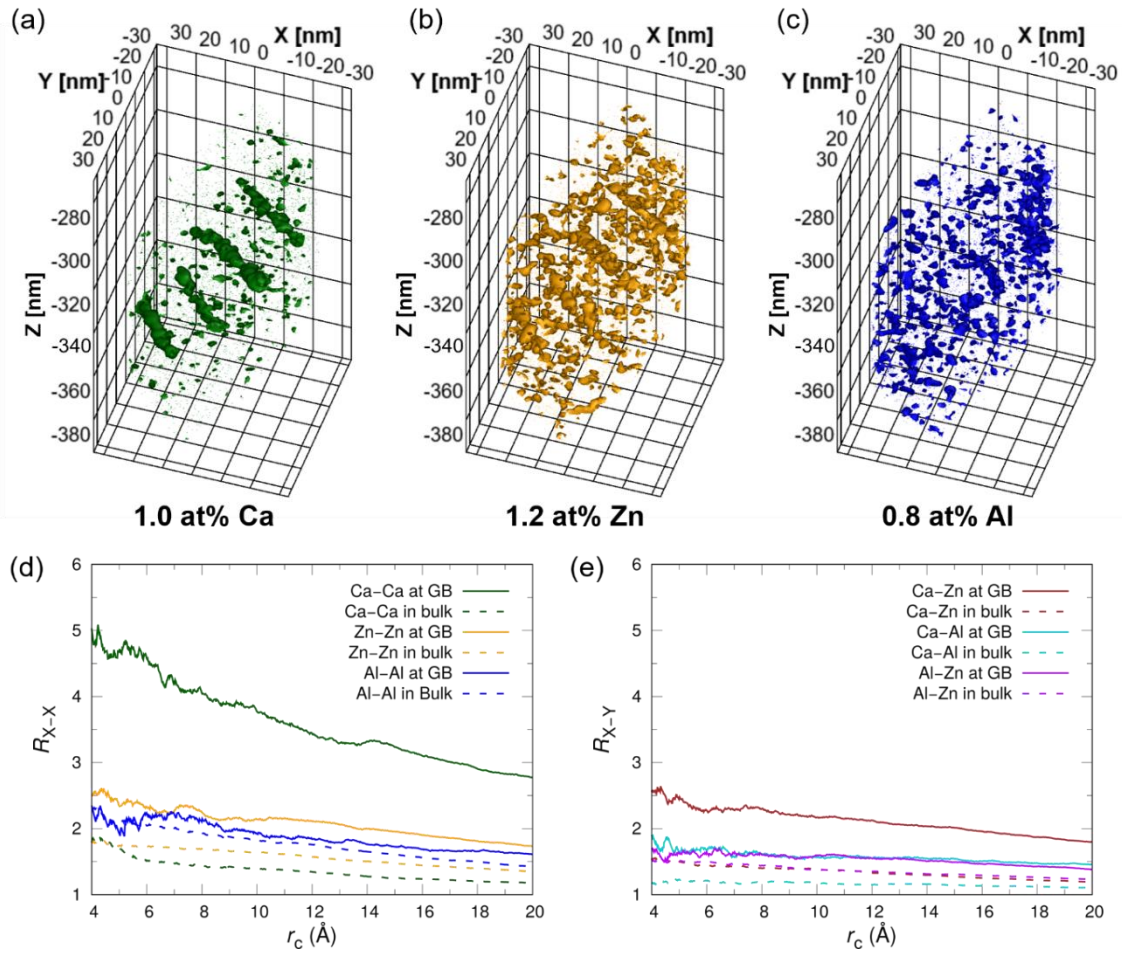


Fig. 2 3D view of the segregation in vicinity of the GB region: (a) Ca atoms overlaid with 1.0 at. % Ca isosurfaces; (b) Zn atoms overlaid 1.2 at. % Zn isosurfaces; (c) Al atoms overlaid 0.8 at. % Al isosurfaces. Clustering tendency of (d) X-X and (e) X-Y pairs at the GB region (with a thickness of 20 nm) and in the bulk region of the APT reconstructed sample.

To understand the reason for the observed inhomogeneous GB segregation behavior, atomistic simulations on a LAGB with experimentally informed characteristics (crystallographic orientation, misorientation angle and GB plane direction) were performed. After structural optimization using the conjugate gradient and FIRE [38, 39] algorithms, a LAGB consisting of an array of edge dislocations with an identical core structure and a spacing of 18.4 nm was obtained (Fig. S 2 (b)). This spacing aligns with the spacing observed in the line segregation structure in experiments and complies with Frank's relation for tilt GB with a  $1^\circ$  misorientation. A cylindrical sample

with a diameter of 18.4 nm, containing one dislocation at the center was extracted to investigate the segregation behavior of solutes. The boundary conditions and swapping region are illustrated in Fig. S 2 (c). For more details on the simulation methods, refer to the Supplementary Material. By substituting one Mg atom with one solute (Ca/Zn/Al) atom near the dislocation core region, the per-site segregation energy  $E_{\text{seg}}$  was calculated according to:

$$E_{\text{seg}} = (\Omega_{\text{GB}} + \Omega_{\text{bulk}}^{\text{X}}) - (\Omega_{\text{GB}}^{\text{X}} + \Omega_{\text{bulk}}),$$

where  $\Omega_{\text{bulk}}$  is the energy of the Mg bulk,  $\Omega_{\text{bulk}}^{\text{X}}$  is the energy of the Mg bulk where one host atom is replaced by a solute,  $\Omega_{\text{GB}}$  is the energy of the Mg system with a GB (or a dislocation), and  $\Omega_{\text{GB}}^{\text{X}}$  is the energy of the Mg system with a solute occupying a GB site. In the above-mentioned definition, a more positive value means a higher tendency of

segregation. After each swap, an energy minimization using the FIRE algorithm was conducted with the force tolerance of  $10^{-8}$  eV/Å.

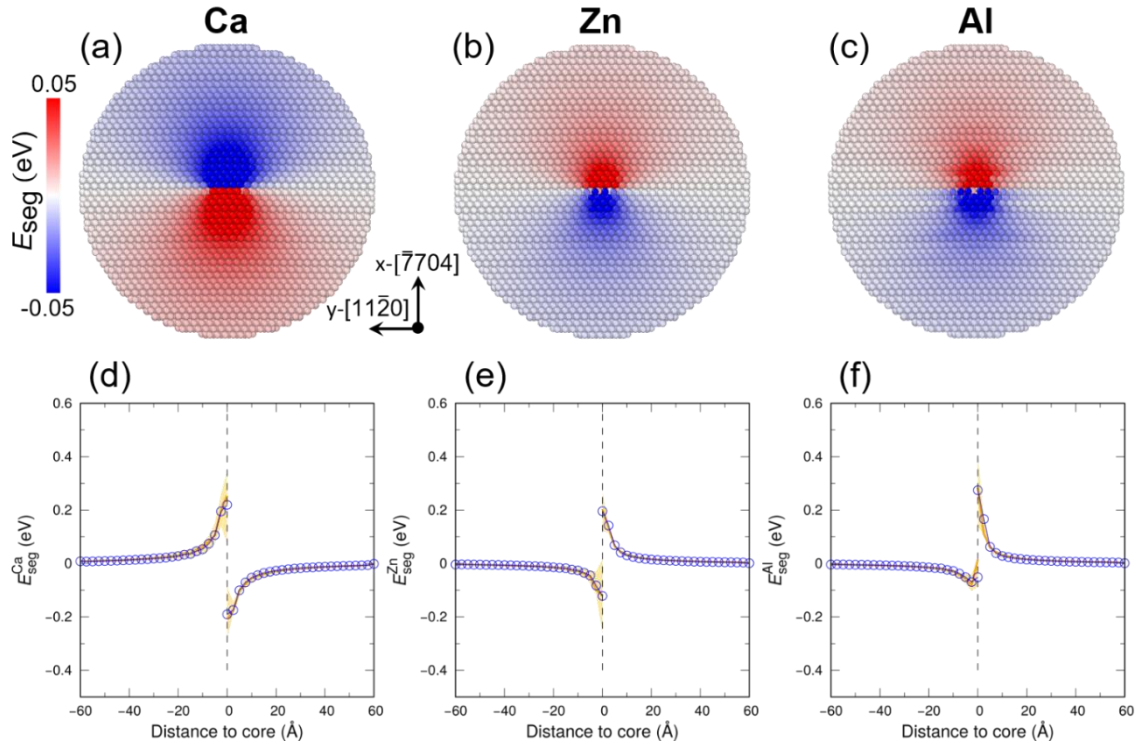


Fig. 3 Atomistic simulations of mono-segregation behavior of (a) Ca, (b) Zn and (c) Al solutes at the dislocation. A positive value indicates that segregation is energetically favorable. The statistics of per-site segregation energies of (d) Ca, (e) Zn and (f) Al solutes as a function of the distance to the center of the dislocation core. The data is divided into bins of  $2.5 \text{ \AA}$ . The upper and lower bounds of the light orange region are third and first quartiles, respectively. The orange line denotes the median values, while the blue dots represent the mean values.

Fig. 3(a-c) shows the distribution of per-site segregation energy of Ca, Zn and Al solutes. Ca solute exhibits a higher tendency to segregate in the tensile stress field (Fig. S 2 (d) and Fig. S 3) due to its larger atomic radius compared to Mg. Conversely, Zn and Al solutes, with smaller atomic radii than Mg, show a greater attraction to sites in the compressive stress field. Although the segregation energies of all three solutes are similar close to the dislocation core (cf. Fig. 3 (d-f)), the distribution of segregation energies for Ca exhibits a much boarder peak compared to the other two solutes. This

distinction becomes more apparent when the per-site segregation energies in each bin are aggregated and plotted against the distance from the dislocation core, as shown in Fig. 4(b). The overall segregation energies of Ca remain consistently higher in the tensile stress field compared to the segregation of Zn and Al in the compressive stress field, extending beyond a distance of 50 Å from the dislocation core. The simulation results on mono-segregation of solutes agree well with the experimental observation of periodic line enrichment of solutes, particularly the Ca solute, at the LAGB.

To gain a deeper understanding of the strong clustering tendency of Ca solutes identified by post-processing the APT data (Fig. 2 (d-e)), the co-segregation of Ca, Zn and Al solutes at the dislocation was modelled in ternary Mg alloys. In this work, only solute-solute pairs within the cutoff of the first nearest neighbor were considered. Fig. 4(a) illustrates multiple energy states ( $\Omega$ ) and differences ( $E$ ) for different co-segregation scenarios [26, 28]. Three energy differences, including co-segregation energies  $E_{\text{coseg}}^{\text{X-Y}}$  and  $E_{\text{coseg}}^{\text{X-Y}}$  and energetic advantages  $\Delta E_{\text{coseg}}^{\text{X-Y}}$  of co-segregation, were calculated to interpret the co-segregation tendency. The co-segregation energy  $E_{\text{coseg}}^{\text{X-Y}}$  was defined as follows:

$$E_{\text{coseg}}^{\text{X-Y}} = (\Omega_{\text{bulk}}^{\text{X}} + \Omega_{\text{bulk}}^{\text{Y}} - 2 \cdot \Omega_{\text{bulk}}) - (\Omega_{\text{GB}}^{\text{X-Y}} - \Omega_{\text{GB}}),$$

where  $\Omega_{\text{GB}}^{\text{X-Y}}$  represents the energy of the Mg system with an X-Y pair occupying two nearby GB sites.  $E_{\text{coseg}}^{\text{X-Y}}$  describes the energy difference when segregating X and Y individually from the bulk and clustering at the GB. The positive  $E_{\text{coseg}}^{\text{X-Y}}$  value implies the solute-solute pair at the GB is more energetically favorable than the separated

solute atoms in the bulk. Another co-segregation energy  $E_{\text{coseg}}^{\text{X-Y}''}$  was computed as follows:

$$E_{\text{coseg}}^{\text{X-Y}''} = (\Omega_{\text{bulk}}^{\text{X-Y}} - \Omega_{\text{bulk}}) - (\Omega_{\text{GB}}^{\text{X-Y}} - \Omega_{\text{GB}}),$$

where  $\Omega_{\text{bulk}}^{\text{X-Y}}$  represents the energy of the Mg bulk where two host atoms are replaced by an X-Y pair.  $E_{\text{coseg}}^{\text{X-Y}''}$  describes the energy difference between X and Y forming a cluster in the bulk and segregating as a cluster at the GB. The positive value indicates that the solute-solute pair at the GB is more energetically favorable than the pair in the bulk. The energetic advantage  $\Delta E_{\text{coseg}}^{\text{X-Y}}$  of co-segregation was computed according to:

$$\Delta E_{\text{coseg}}^{\text{X-Y}} = E_{\text{coseg}}^{\text{X-Y}''} - (E_{\text{seg}}^{\text{X}} + E_{\text{seg}}^{\text{Y}}),$$

where a positive value indicates the co-segregation of an X-Y pair is more energetically favorable than the mono-segregation of X and Y solutes separately at the GB.

The co-segregation behavior of solute-solute pairs at the dislocation core region is shown in Fig. 4(c-e) and Fig. S 4-6. The scenario of segregation of separate solute atoms and clustering at the GB was investigated, as shown in Fig. 4 (c). For Ca-Ca pairs, the  $E_{\text{coseg}}^{\text{X-Y}'}$  values predominantly remain negative, except for a small region within a distance of 10 Å from the dislocation core in the tensile stress field. For Zn-Zn, Al-Al, and Al-Zn pairs, the  $E_{\text{coseg}}^{\text{X-Y}'}$  values are positive within the distances of 12.5, 40 and 20 Å from the dislocation core in the compressive stress field. Regarding Ca-Zn and Ca-Al pairs, the  $E_{\text{coseg}}^{\text{X-Y}'}$  values decrease and approach zero as the distance to the dislocation core decreases, which indicates the segregation of these separate solutes and clustering at the dislocation becomes less favorable closer to the defect.

For the co-segregation of solute-solute pairs from the bulk, Ca-Ca, Ca-Zn and Ca-Al pairs are more favorable in the tensile stress field of the dislocation (Fig. 4(d)).

In contrast, Zn-Zn, Al-Al and Zn-Al pairs demonstrate a preference for segregation in the compressive stress field, following a similar trend. Among all solute-solute pairs, the distribution of co-segregation energies  $E_{\text{coseg}}^{\text{X-Y}}$  of Ca-Ca pair remains consistently high and extends beyond a distance of 50 Å from the dislocation core in the tensile stress field. Moreover, Ca-Zn and Ca-Al pairs exhibit a similar trend, as the presence of Ca enhances the propensity of Zn and Al solutes to segregate in the tensile stress field, which is unfavorable for the mono-segregation of these elements.

Fig. 4(e) shows the energetic advantages  $\Delta E_{\text{coseg}}^{\text{X-Y}}$  of co-segregation for solute-solute pairs compared to the mono-segregation of individual solutes at the dislocation. The  $\Delta E_{\text{coseg}}^{\text{Ca-Ca}}$  values exhibit a positive trend, ranging from 20 Å in the tensile stress field to 5 Å in the compressive stress field, indicating that the clustering of Ca solutes near the dislocation core is energetically favorable. Conversely, the  $\Delta E_{\text{coseg}}^{\text{X-Y}}$  values for other pairs predominantly remain negative, suggesting that the clustering of solute-solute pairs other than Ca-Ca pair is not favorable at the dislocation core. This finding aligns well with the pronounced tendency for Ca-Ca clustering compared to other pairs, ranging from short to long-range orders, as observed from the APT clustering analysis.



range of the tensile stress field ( $> 50 \text{ \AA}$ ), which agrees with the APT-measured solute distribution at the LAGB. In contrast, the segregation of separate Ca solutes and clustering at the GB is only favorable in a narrow range of the tensile stress field ( $< 10 \text{ \AA}$ ). In comparison to the  $E_{\text{coseg}}^{\text{X-Y} \prime}$  scenario, the co-segregation energy of solute-solute pairs  $E_{\text{coseg}}^{\text{X-Y} \prime \prime}$  may offer a more plausible explanation for the co-segregation behavior observed at the LAGB in the chemical complex Mg alloy. As the solute concentration at the LAGB increases, the energy advantage of co-segregation over separate mono-segregation at the GB  $\Delta E_{\text{coseg}}^{\text{X-Y}}$  becomes relevant for interpreting clustering tendency. The high  $\Delta E_{\text{coseg}}^{\text{Ca-Ca}}$  values at the dislocation core region rationalize the experimental observation of predominant Ca-Ca clustering at the LAGB. It is worth mentioning that the co-segregation behavior is also influenced by other important factors, such as chemical potential and diffusion mechanisms.

The segregation of solute elements to the dislocation array minimizes the system's free energy according to the Gibbs adsorption isotherm [40]. Structural transitions driven by solute segregation at the line defects were reported in Mg-Zn [20] and Fe-Mn [41] alloys with relatively high solute concentrations and interpreted in terms of dislocation defect phases [42]. Given the low solute concentrations (0.21 at.% Al, 0.23 at.% Ca and 0.61 at.% Zn in the Mg alloy) therefore low solute chemical potentials, it is expected that the periodic line defects would be decorated metastable states rather than exothermic defect phases. High-resolution techniques are required to characterize the atomic structures and chemical short-range orders of the dislocation defect states. According to classic recrystallization theory, LAGB movement plays a key role in the process of recrystallization nucleation before it transforms into HAGB by a mechanism of vacancy-mediated climb of dislocations [11, 13, 43]. Solute atoms segregating on LAGB could execute an additional attraction on the vacancies,



hindering their diffusion and the climbing of extrinsic dislocations pinning the intrinsic dislocations on the LAGB [10, 11, 13, 43]. Higher magnitude of segregation of Ca and Zn or Al was therefore observed to significantly restricted recrystallization nucleation in magnesium alloys [10, 44]. To fully understand the role of inhomogeneous segregation in the texture modification during dynamic or static recrystallizations, segregation behaviors on wider range of LAGBs should be further measured and simulated in Ca- or RE- containing magnesium alloys.

In summary, we used atomic-scale experimental and modelling techniques to investigate the co-segregation behavior of Ca, Zn, and Al solutes at a LAGB in a chemical complex Mg alloy. By employing 3D APT and subsequent clustering analysis, we revealed a pronounced tendency for Ca solutes to cluster at the dislocation array. Solute-solute pair segregation was identified as a plausible co-segregation scenario using atomistic simulations. Furthermore, the modelling suggests that the co-segregation of Ca-Ca pairs near the dislocation core region is energetically more favorable compared to other solutes and solute-solute pairs, which rationalizes the experimental observation of pronounced Ca enrichment and clustering at the LAGB.

## **Acknowledgements**

R.P. and T.A.S. are grateful for the financial support from the German Research Foundation (DFG) (Grant Nr. AL1343/7-1, AL1343/8-1 and Yi 103/3-1). Z.X. and T.A.S. acknowledge the financial support by the DFG (Grant Nr. 505716422). Z.X. and S.K.K. acknowledge financial support by the DFG through the projects A02, A05 and C02 of the SFB1394 Structural and Chemical Atomic Complexity – From Defect Phase Diagrams to Material Properties, project ID 409476157. Additionally, Z.X. and S.K.K. are grateful for funding from the European Research Council (ERC) under the

European Union's Horizon 2020 research and innovation programme (grant agreement No. 852096 FunBlocks). J.G. acknowledges funding from the French National Research Agency (ANR), Grant ANR-21-CE08-0001 (ATOUUM) and ANR-22-CE92-0058-01 (SILA). The authors gratefully acknowledge the computing time provided to them at the NHR Center NHR4CES at RWTH Aachen University (project number p0020267). This is funded by the Federal Ministry of Education and Research, and the state governments participating on the basis of the resolutions of the GWK for national high performance computing at universities ([www.nhr-verein.de/unsere-partner](http://www.nhr-verein.de/unsere-partner)).

## Supplementary Material

### Methods

#### APT characterization

To assess the clustering tendency of various elements in the APT reconstructed sample, a clustering ratio parameter  $R_{A-B}$  [45] is utilized. This  $R_{A-B}$  ratio compares the number of a particular element within a specific cutoff distance to the expected number of that element in a homogeneous distribution within the same cutoff. Assuming a homogeneous distribution of B atoms throughout the sample, the ideal number of B atoms in a cutoff distance  $r$  can be calculated using the following equation:

$$N_{B,\text{homo}}(r) = \frac{4}{3}\pi r^3 \frac{N_B}{V},$$

where  $N_{A-B}(r)$  is the number of B atoms surrounding an A site within a cutoff distance  $r$  (excluding the B atom on the A site) and  $N_A$  is the number of A sites. From that, the clustering ratio  $R_{A-B}$  is defined as:

$$\bar{N}_{A-B}(r) = \frac{\sum_{N_A} N_{A-B}(r)}{N_A},$$

where  $N_{A-B}(r)$  is the number of B atoms surrounding an A site within a cutoff distance  $r$  and  $N_A$  is the number of A sites. From that, the clustering ratio  $R_{A-B}$  is defined as:

$$R_{A-B} = \frac{\bar{N}_{A-B}(r)}{N_{B,\text{homo}}(r)},$$

if  $R_{A-B} = 1$ , the distribution of B atoms surrounding the A site within a cutoff distance  $r$  is considered homogeneous. The APT reconstructed samples were divided into two regions: a GB region, with a thickness of 20 nm along the GB, and the remaining samples were considered as the bulk region. To calculate the  $R_{A-B}$  values for the GB

and bulk regions, as well as for the entire sample, we normalized using  $N_{B,homo,bulk}(r)$  which was obtained based on the number of B atoms,  $N_{B,bulk}$ , and volume,  $V_{bulk}$ , of the bulk region.

## Atomistic simulations

To explain the strong clustering tendency of Ca solutes observed at the dislocation array, atomistic simulations were conducted using LAMMPS [31] in conjunction with the modified embedded atom method (MEAM) potentials for MgCaZn [32], MgCaAl and MgZnAl [23]. The potential properties of the Mg matrix, including elastic constants, stacking fault and grain boundary energies, agree well with the experimental and ab-initio values [24]. The per-site segregation energy of Ca, Zn and Al solutes at  $\Sigma 7$   $21.8^\circ$   $\{12\bar{3}0\}\langle 0001\rangle$  grain boundary,  $\{10\bar{1}1\}$  and  $\{10\bar{1}2\}$  twin boundaries were calculated and compared with the ab-initio calculations [21, 22]. The results illustrated in Table S1 indicate that the potentials have can reasonably describe the segregation behavior of individual solutes at the Mg grain boundaries, aligning well with the ab-initio results. The atomic configuration of the symmetric tilt LAGB were constructed using AtomsK [34] based on the experimentally-informed crystallographic orientations of two grains and the GB plane (normal to the y-axis) obtained from TKD grain mapping and reconstructed APT tips. The simulation setup is illustrated in Fig. S 2. The microscopic degrees of freedom of the symmetric tilt LAGB were explored by performing rigid body shift and structural relaxation using FIRE algorithm [38, 39] normal to the GB plane. A 2D cylindrical setup with a radius of 18.4 nm was cut out in the fully relaxed sample to investigate the segregation behavior at the dislocation, as shown in Fig. S 2 (b-c). The outermost layers of the cylindrical surface with a thickness of 1.2 nm (2 times interatomic potential cutoff) were fixed in x and y directions. Periodic boundary conditions were applied along the dislocation line (z-) direction. The effect of

the boundary conditions on the calculated per-site segregation energy is negligible (less than 0.1 meV). The Open Visualization Tool OVITO [46] was used to visualize the atomistic configurations.

Table S 1 Segregation energies (in eV) of Ca, Zn and Al solutes at Mg  $\Sigma 7$   $21.8^\circ \{12\bar{3}0\} \langle 0001 \rangle$  grain boundary (T-type),  $\{10\bar{1}1\}$  and  $\{10\bar{1}2\}$  twin boundaries calculated using the MEAM potentials. Bold values indicate a structural transition took place.

GB type	Site	Ca		Zn		Al	
		MEAM	DFT[21, 22]	MEAM	DFT[21, 22]	MEAM	DFT[21, 22]
$\Sigma 7$ -T	a1	-0.21	-0.31	0.16	0.26	0.25	0.18
$\Sigma 7$ -T	a2	-0.04	0.11	0.05	0.01	0.01	-0.02
$\Sigma 7$ -T	a3	0.40	0.73	-0.27	-0.34	-0.43	-0.33
$\Sigma 7$ -T	b	<b>-0.05</b>	-0.07	0.16	0.3	0.21	0.15
$\Sigma 7$ -T	c	0.08	0.02	-0.02	0.01	-0.01	-0.02
$\Sigma 7$ -T	d	0.20	0.30	-0.04	0.03	<b>0.01</b>	-0.03
$\Sigma 7$ -T	e	<b>-0.03</b>	<b>0.11</b>	0.14	0.19	<b>0.20</b>	0.12
$\{10\bar{1}1\}$	A	-0.18	-0.327	0.163	0.231	0.236	0.162
$\{10\bar{1}1\}$	B	0.19	0.116	-0.161	-0.150	-0.216	-0.117
$\{10\bar{1}2\}$	A1	<b>0.00</b>	-	0.220	0.228	0.269	0.146
$\{10\bar{1}2\}$	B1	0.25	0.30	<b>-0.018</b>	-0.143	<b>-0.012</b>	-0.114

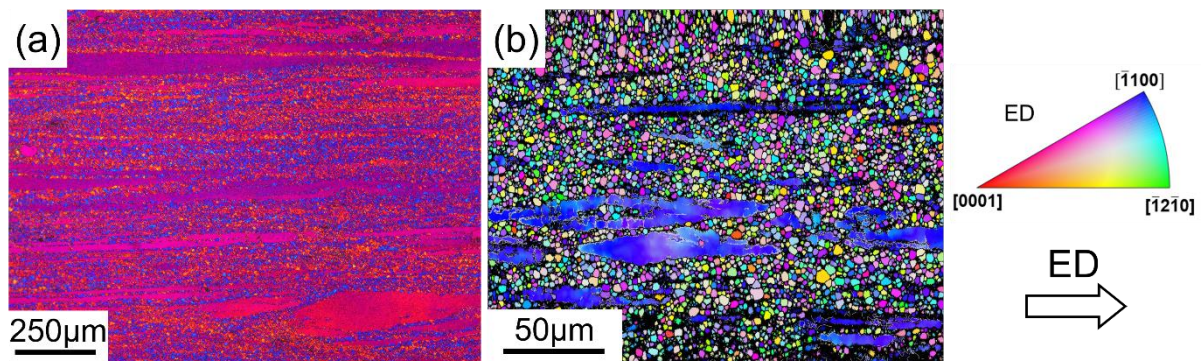


Fig. S 1 Microstructure of as-extruded AZX alloy: (a) optical microscopic image; (b) EBSD map with IPF color key along ED.

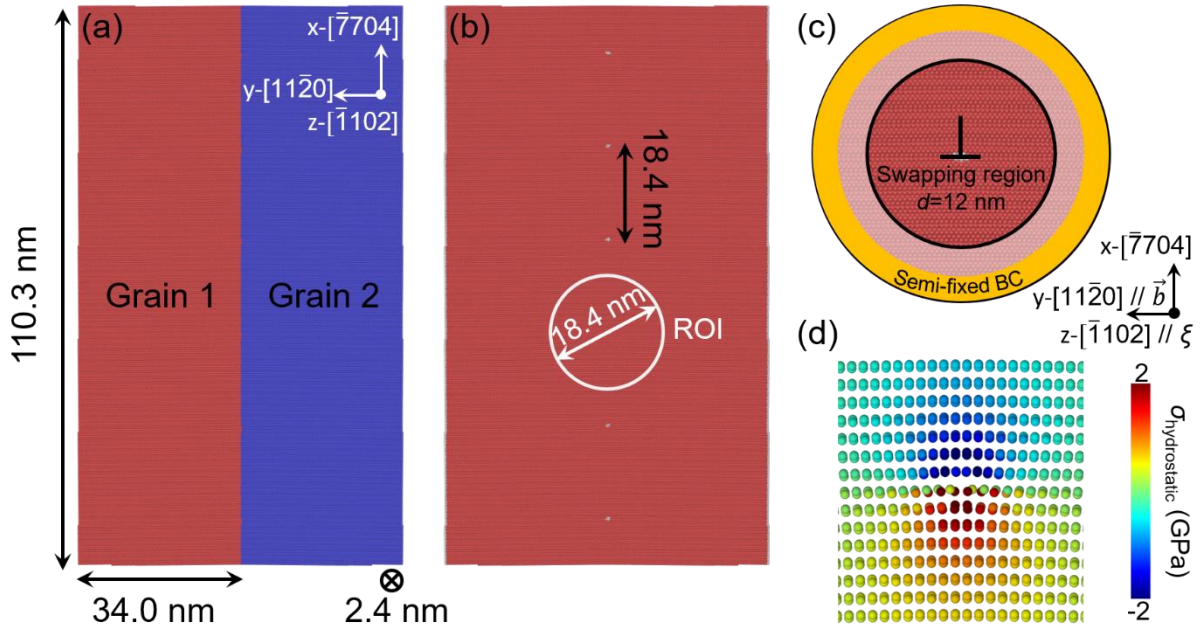


Fig. S 2 Atomistic configuration of the symmetric tilt low-angle grain boundary (LAGB) with a misorientation of  $1^\circ$  along  $[\bar{1}10\bar{2}]$  axis on  $(11\bar{2}0)$  plane in Mg. (a) Slab setup ( $110.3 \times 68.0 \times 2.4 \text{ nm}^3$ ) of the symmetric tilt LAGB with periodic boundary conditions in x and z directions. (b) The symmetric tilt LAGB after relaxation consisted of an array of edge dislocations with an identical core structure and a spacing of 18.4 nm. Atoms are colored according to the common neighbor analysis [43], where atoms at the dislocation cores are shown in white. (c) Schematic of the cylindrical setup ( $d=18.4 \text{ nm}$ ,  $l_z=2.4 \text{ nm}$ ) for solute segregation calculation at the dislocation with semi-fixed boundary conditions (constrained in x and y directions) at the outermost layers with a thickness of 1.4 nm. (d) Hydrostatic stress map of the dislocation core region, where blue and red regions represent compressive and tensile stress fields of the edge dislocation.

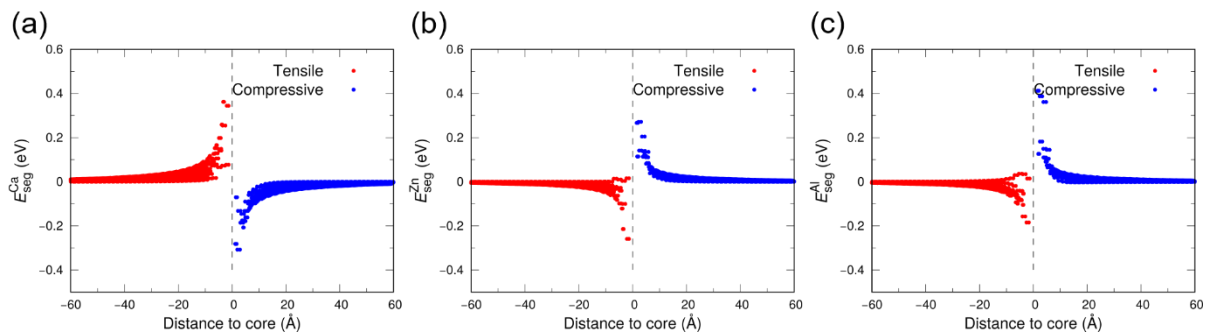


Fig. S 3 Distributions of per-site segregation energies  $E_{\text{seg}}^X$  of (a) Ca, (b) Zn and (c) Al solutes as a function of the distance to the center of the dislocation core.

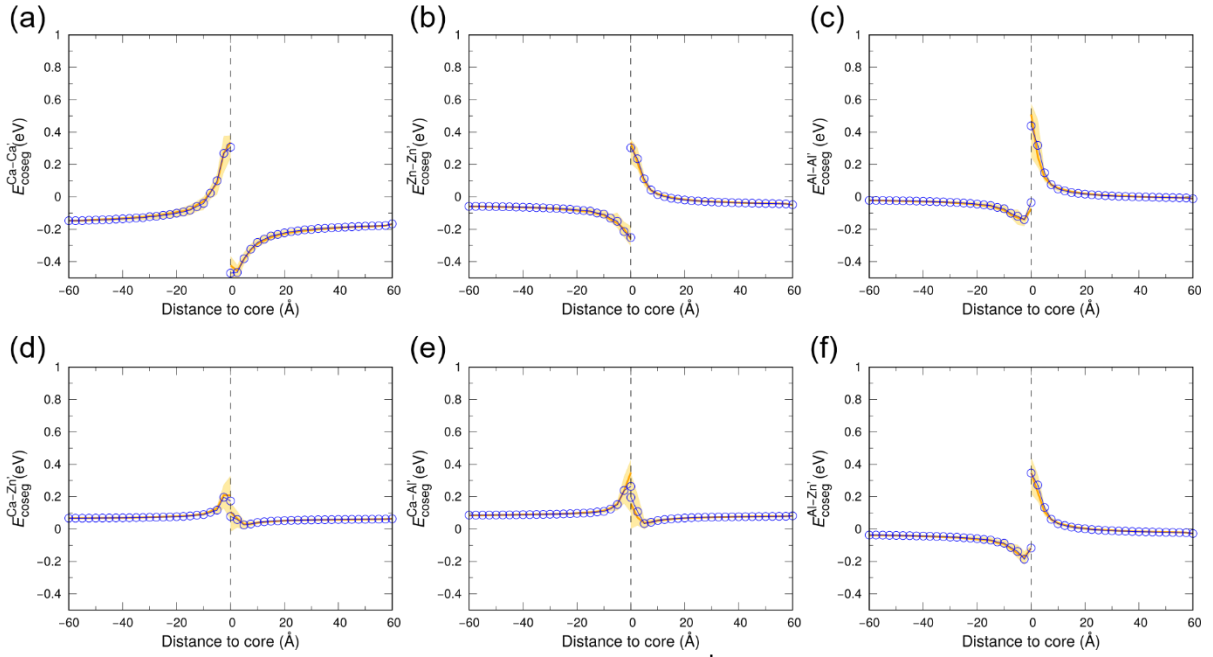


Fig. S 4 The statistics of co-segregation energies  $E_{coseg}^{X-Y}$  of (a) Ca-Ca, (b) Zn-Zn, (c) Al-Al, (d) Ca-Zn, (e) Ca-Al and (f) Al-Zn pairs as a function of the distance to the center of the dislocation core. The data is divided into bins of 2.5 Å. The upper and lower bounds of the light orange region are third and first quartiles, respectively. The orange line denotes the median values, while the blue dots represent the mean values.

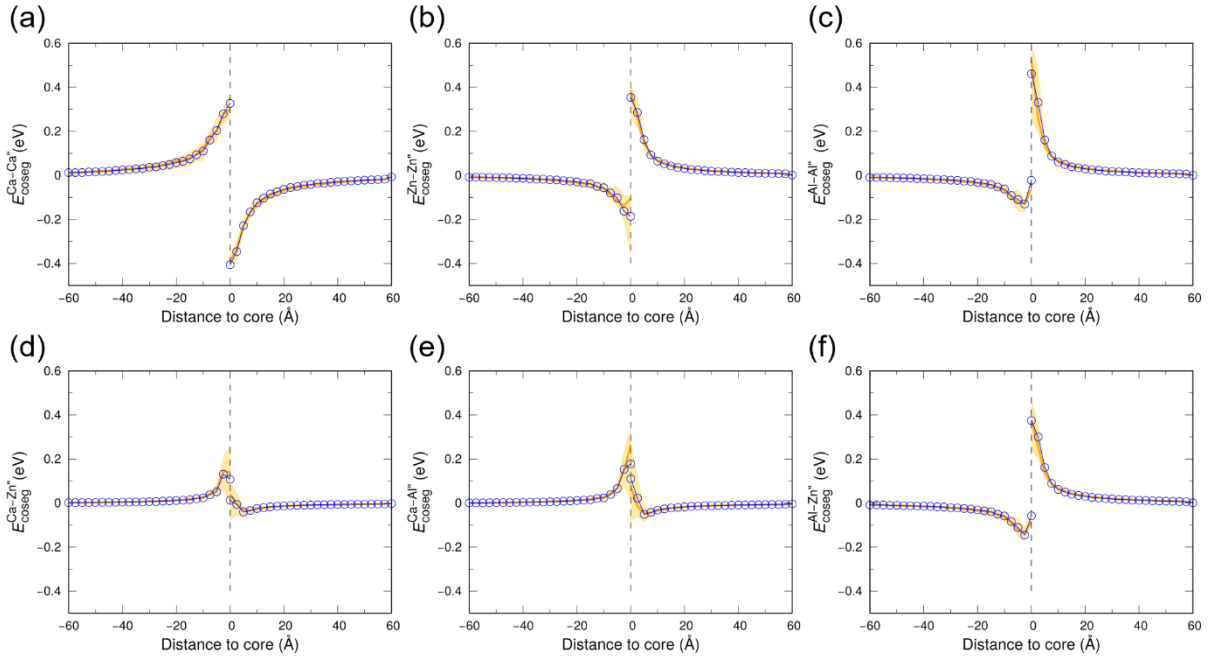


Fig. S 5 The statistics of co-segregation energies  $E_{coseg}^{X-Y}$  of (a) Ca-Ca, (b) Zn-Zn, (c) Al-Al, (d) Ca-Zn, (e) Ca-Al and (f) Al-Zn pairs as a function of the distance to the center of the dislocation core. The data is divided into bins of 2.5 Å. The upper and lower bounds of the light orange

region are third and first quartiles, respectively. The orange line denotes the median values, while the blue dots represent the mean values.

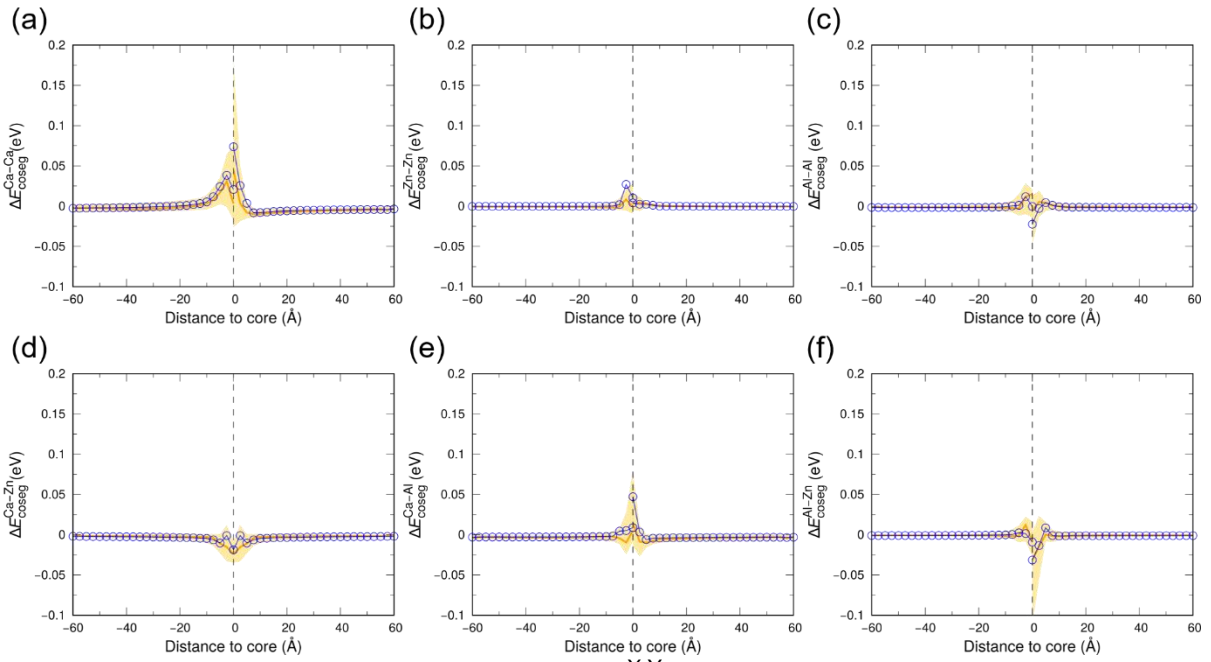


Fig. S 6 The statistics of energetic advantage  $\Delta E_{\text{coseg}}^{X-Y}$  of co-segregation of (a) Ca-Ca, (b) Zn-Zn, (c) Al-Al, (d) Ca-Zn, (e) Ca-Al and (f) Al-Zn pairs as a function of the distance to the center of the dislocation core. The data is divided into bins of 2.5 Å. The upper and lower bounds of the light orange region are third and first quartiles, respectively. The orange line denotes the median values, while the blue dots represent the mean values.



## References

- [1] I. Basu, T. Al-Samman, G. Gottstein, Shear band-related recrystallization and grain growth in two rolled magnesium-rare earth alloys, *Mater. Sci. Eng., A* 579 (2013) 50-56.
- [2] I. Basu, T. Al-Samman, Triggering rare earth texture modification in magnesium alloys by addition of zinc and zirconium, *Acta Mater.* 67 (2014) 116-133.
- [3] C.W. Su, L. Lu, M.O. Lai, Recrystallization and grain growth of deformed magnesium alloy, *Philos. Mag.* 88(2) (2008) 181-200.
- [4] H.J. McQueen, Development of dynamic recrystallization theory, *Mater. Sci. Eng., A* 387 (2004) 203-208.
- [5] K.J. Tam, M.W. Vaughan, L. Shen, M. Knezevic, I. Karaman, G. Proust, Modelling dynamic recrystallisation in magnesium alloy AZ31, *Int. J. Plast.* 142 (2021) 102995.
- [6] K. Huang, R.E. Logé, A review of dynamic recrystallization phenomena in metallic materials, *Materials & Design* 111 (2016) 548-574.
- [7] Y. Cai, C.Y. Sun, Y.L. Li, S.Y. Hu, N.Y. Zhu, E.I. Barker, L.Y. Qian, Phase field modeling of discontinuous dynamic recrystallization in hot deformation of magnesium alloys, *Int. J. Plast.* 133 (2020) 102773.
- [8] S.E. Ion, F.J. Humphreys, S.H. White, DYNAMIC RECRYSTALLIZATION AND THE DEVELOPMENT OF MICROSTRUCTURE DURING THE HIGH-TEMPERATURE DEFORMATION OF MAGNESIUM, *Acta Metall.* 30(10) (1982) 1909-1919.
- [9] M. Stipp, H. Stunitz, R. Heilbronner, S.M. Schmid, The eastern Tonale fault zone: a 'natural laboratory' for crystal plastic deformation of quartz over a temperature range from 250 to 700 degrees C, *Journal of Structural Geology* 24(12) (2002) 1861-1884.
- [10] R. Pei, Y. Zou, M. Zubair, D. Wei, T. Al-Samman, Synergistic effect of Y and Ca addition on the texture modification in AZ31B magnesium alloy, *Acta Materialia* 233 (2022) 117990.
- [11] M. Winning, A.D. Rollett, G. Gottstein, D.J. Srolovitz, A. Lim, L.S. Shvindlerman, Mobility of low-angle grain boundaries in pure metals, *Philosophical Magazine* 90(22) (2010) 3107-3128.
- [12] D.G. Cram, X.Y. Fang, H.S. Zurob, Y.J.M. Bréchet, C.R. Hutchinson, The effect of solute on discontinuous dynamic recrystallization, *Acta Mater.* 60(18) (2012) 6390-6404.
- [13] C. Antonione, G.D. Gatta, A. Lucci, G. Riontino, G. Venturello, The role of substitutional transition elements on recrystallization processes in dilute iron solid solutions, *Acta Metallurgica* 18(11) (1970) 1169-1180.
- [14] H. Xie, Q. Huang, J. Bai, S. Li, Y. Liu, J. Feng, Y. Yang, H. Pan, H. Li, Y. Ren, G. Qin, Nonsymmetrical Segregation of Solute in Periodic Misfit Dislocations Separated Tilt Grain Boundaries, *Nano Lett.* 21(7) (2021) 2870-2875.
- [15] H. Xie, H. Pan, J. Bai, D. Xie, P. Yang, S. Li, J. Jin, Q. Huang, Y. Ren, G. Qin, Twin Boundary Superstructures Assembled by Periodic Segregation of Solute Atoms, *Nano Lett.* 21(22) (2021) 9642-9650.
- [16] M. Bugnet, A. Kula, M. Niewczas, G.A. Botton, Segregation and clustering of solutes at grain boundaries in Mg-rare earth solid solutions, *Acta Mater.* 79 (2014) 66-73.
- [17] J.F. Nie, Y.M. Zhu, J.Z. Liu, X.Y. Fang, Periodic Segregation of Solute Atoms in Fully Coherent Twin Boundaries, *Science* 340(6135) (2013) 957-960.
- [18] Y.M. Zhu, M.Z. Bian, J.F. Nie, Tilt boundaries and associated solute segregation in a Mg-Gd alloy, *Acta Mater.* 127 (2017) 505-518.
- [19] M. Bugnet, A. Kula, M. Niewczas, G.A. Botton, Segregation and clustering of solutes at grain boundaries in Mg-rare earth solid solutions, *Acta Mater.* 79 (2014) 66-73.
- [20] Z. Yang, L. Zhang, M.F. Chisholm, X. Zhou, H. Ye, S.J. Pennycook, Precipitation of binary quasicrystals along dislocations, *Nature Communications* 9(1) (2018) 809.
- [21] L. Huber, J. Rottler, M. Militzer, Atomistic simulations of the interaction of alloying elements with grain boundaries in Mg, *Acta Materialia* 80 (2014) 194-204.
- [22] Z. Pei, R. Li, J.-F. Nie, J.R. Morris, First-principles study of the solute segregation in twin boundaries in Mg and possible descriptors for mechanical properties, *Materials & Design* 165 (2019) 107574.
- [23] J. Messina, R. Luo, K. Xu, G. Lu, H. Deng, M.A. Tschopp, F. Gao, Machine learning to predict aluminum segregation to magnesium grain boundaries, *Scripta Materialia* 204 (2021) 114150.
- [24] R. Pei, Z. Xie, S. Yi, S. Korte-Kerzel, J. Guérolé, T. Al-Samman, Atomistic insights into the inhomogeneous nature of solute segregation to grain boundaries in magnesium, *Scripta Materialia* 230 (2023) 115432.
- [25] C.L. White, W.A. Coghlan, The spectrum of binding energies approach to grain boundary segregation, *Metallurgical Transactions A* 8(9) (1977) 1403-1412.

- [26] C. Elsässer, T. Elsässer, Codoping and Grain-Boundary Cosegregation of Substitutional Cations in  $\alpha$ -Al<sub>2</sub>O<sub>3</sub>: A Density-Functional-Theory Study, *Journal of the American Ceramic Society* 88(1) (2005) 1-14.
- [27] D.A. Aksyonov, T. Hickel, J. Neugebauer, A.G. Lipnitskii, The impact of carbon and oxygen in alpha-titanium: ab initio study of solution enthalpies and grain boundary segregation, *Journal of Physics: Condensed Matter* 28(38) (2016) 385001.
- [28] D. Scheiber, L. Romaner, R. Pippan, P. Puschnig, Impact of solute-solute interactions on grain boundary segregation and cohesion in molybdenum, *Physical Review Materials* 2(9) (2018) 093609.
- [29] A. Ahmadian, D. Scheiber, X. Zhou, B. Gault, C.H. Liebscher, L. Romaner, G. Dehm, Aluminum depletion induced by co-segregation of carbon and boron in a bcc-iron grain boundary, *Nature Communications* 12(1) (2021) 6008.
- [30] M. Wagih, C.A. Schuh, Viewpoint: Can symmetric tilt grain boundaries represent polycrystals?, *Scripta Materialia* 237 (2023) 115716.
- [31] A.P. Thompson, H.M. Aktulga, R. Berger, D.S. Bolintineanu, W.M. Brown, P.S. Crozier, P.J. in 't Veld, A. Kohlmeyer, S.G. Moore, T.D. Nguyen, R. Shan, M.J. Stevens, J. Tranchida, C. Trott, S.J. Plimpton, LAMMPS - a flexible simulation tool for particle-based materials modeling at the atomic, meso, and continuum scales, *Comput. Phys. Commun.* 271 (2022) 108171.
- [32] H.-S. Jang, D. Seol, B.-J. Lee, Modified embedded-atom method interatomic potential for the Mg–Zn–Ca ternary system, *Calphad* 67 (2019) 101674.
- [33] H.-S. Jang, D. Seol, B.-J. Lee, Modified embedded-atom method interatomic potentials for Mg–Al–Ca and Mg–Al–Zn ternary systems, *Journal of Magnesium and Alloys* 9(1) (2021) 317-335.
- [34] P. Hirel, AtomsK: A tool for manipulating and converting atomic data files, *Comput. Phys. Commun.* 197 (2015) 212-219.
- [35] M. Schreiber, K.D. Molodov, T. Al-Samman, D.A. Molodov, On the role and alteration of grain boundaries in/during accommodating plasticity in magnesium, *Acta Mater.* 191 (2020) 124-130.
- [36] B.A. Bilby, Bristol conference report on defects in crystalline materials, *Phys. Soc.* (1955) 123.
- [37] F.C. Frank, The resultant content of dislocations in an arbitrary intercrystalline boundary, *Symposium on the Plastic Deformation of Crystalline Solids* (1950) 150-154.
- [38] E. Bitzek, P. Koskinen, F. Gähler, M. Moseler, P. Gumbsch, Structural Relaxation Made Simple, *Phys. Rev. Lett.* 97(17) (2006) 170201.
- [39] J. Guérolé, W.G. Nöhring, A. Vaid, F. Houllé, Z. Xie, A. Prakash, E. Bitzek, Assessment and optimization of the fast inertial relaxation engine (fire) for energy minimization in atomistic simulations and its implementation in lammmps, *Computational Materials Science* 175 (2020) 109584.
- [40] C.L. Briant, Grain boundary segregation in metals, *Proceedings, annual meeting, Electron Microscopy Society of America* 50 (1992) 1204-1205.
- [41] A. Kwiatkowski da Silva, D. Ponge, Z. Peng, G. Inden, Y. Lu, A. Breen, B. Gault, D. Raabe, Phase nucleation through confined spinodal fluctuations at crystal defects evidenced in Fe-Mn alloys, *Nature Communications* 9(1) (2018) 1137.
- [42] S. Korte-Kerzel, T. Hickel, L. Huber, D. Raabe, S. Sandlöbes-Haut, M. Todorova, J. Neugebauer, Defect phases – thermodynamics and impact on material properties, *International Materials Reviews* 67(1) (2022) 89-117.
- [43] J.D. Honeycutt, H.C. Andersen, Molecular dynamics study of melting and freezing of small Lennard-Jones clusters, *The Journal of Physical Chemistry* 91(19) (1987) 4950-4963.
- [44] R. Pei, Y. Zou, D. Wei, T. Al-Samman, Grain boundary co-segregation in magnesium alloys with multiple substitutional elements, *Acta Materialia* 208 (2021) 116749.
- [45] A. Tilocca, A.N. Cormack, N.H. de Leeuw, The Structure of Bioactive Silicate Glasses: New Insight from Molecular Dynamics Simulations, *Chemistry of Materials* 19(1) (2007) 95-103.
- [46] A. Stukowski, Visualization and analysis of atomistic simulation data with OVITO—the Open Visualization Tool, *Modell. Simul. Mater. Sci. Eng.* 18(1) (2009) 015012.